IJMF, Iranian Journal of Materials Forming, Vol. 1, No. 2, pp 32-43
Printed in The Islamic Republic of Iran, 2014

Dynamic Recrystallization Kinetics of AISI 403 Stainless Steel Using Hot Compression Test

E. Kevanlo[1], G.R. Ebrahimi[2*], S.A.A. Sani[3] and A. Momeni[4]

[1,2]Department of Materials and Polymer Engineering, Hakim Sabzevari University, Sabzevar, Iran
[3]Department of Materials Science and Engineering, Iran University of Sience and Technology, Tehran, Iran
[4]Department of Materials Science and Engineering, Hamedan University of Technology, Hamedan, Iran

Abstract: In this work dynamic recrystallization behavior of AISI 403 martensitic stainless steel was studied using hot compression tests over temperature range of 900°C -1200°C and strain rate range of 0.001 s^{-1}-1 s^{-1}. The obtained flow curves showed that the hot compression behavior of the alloy is controlled by dynamic recrystallization. The flow stress and strain corresponding to the critical, peak and onset of steady state region were related to the Zener-Hollomon parameter using simple power equations. The variation of dynamic recrystallization fraction with strain showed that restoration kinetics is enhanced with increasing the temperature and decreasing the strain rate. The development of DRX was modeled using Avrami Kinetics equation. The equations proposed by Baragar and Cingara-McQueen were used to develop a new model capable of predicting the flow curves up to the onset of steady state flow region. This softening work is mainly controlled by the phenomenon of dynamic recrystallization.

Keywords: Martensitic-stainless steel, Dynamic recrystallization, Hot deformation, Recrystallization kinetics

1. Introduction

Dynamic recrystallization (DRX) is very crucial to the microstructural evolution during hot deformation of alloys with low and medium stacking fault energy (SFE) [1-4]. This phenomenon changes the microstructure substantially through nucleation and growth of new strain-free grains at the expense of pre-existing work hardened ones. In the low and medium SFE materials, the nucleation mechanism mainly comprises grain boundary bulging which is often referred to as strain induced grain boundary migration (SIBM). Different dislocation densities at the two sides of a grain boundary provide the required driving force for SIBM [5]. The bulged boundaries then sweep away the dislocations evolving initial structure into the new dislocation free, or the low dislocation density one. Based on the mentioned underlying phenomena, DRX is of critical importance from the industrial viewpoint because it reduces the stored strain energy and the corresponding softening effect decreases the required force to shape a work piece. Taking the advantage of DRX to decrease the required energy for shaping a product as well as avoiding plastic instabilities or premature fracture is quite a practical way in different industrial processes, e.g. hot forging [6]. In addition to this, DRX often contributes to improving microstructure, thereby refining the grain structure and improving the mechanical properties of the industrial parts.

The practical and scientific importance of DRX signifies the extensive investigations done in the past decades to predict its condition and kinetics in different alloys [7-11]. It has been well-known that the required conditions for the initiation and completion of dynamic recrystallization depend on the materials parameters such as chemical composition and the processing variables, temperature and strain rate.

Received by the editors August 19, 2014; Revised October 7, 2014 and Accepted October 9, 2014.
*Corresponding author (ebrahimi@hsu.ac.ir)

Therefore, for a careful design of hot working operation, having an in-depth knowledge about the dynamic recrystallization behavior of the material is very essential. The influence of chemical composition is also crucial in view of the precipitation of second phases and its interaction with DRX. In a recent work done on 403 and 403Nb alloys, it has been confirmed that DRX simply comes into operation in the former alloy unlike to the latter one [12]. The inhibition of DRX can be attributed to the pinning effect of Niobium carbides on the grain boundaries.

The physical simulation technique using hot compression tests is a common way of assessing the DRX behavior of a material at various deformation conditions. Moreover, it is possible to investigate hot deformation behavior over a variety of conditions using mathematical equations based on Zener-Holloman parameter [13]. Mathematical equations can also be applied to calculate the changes in recrystallized fraction during hot deformation [14]. The experimental techniques have been widely used for different types of stainless steels, in order to develop useful experimental equations [15]. These equations are applicable to generalize the laboratory results to the industrial hot working operations. Despite the extensive works done on the hot deformation behavior of stainless steels, the martensitic grades have received less attention. Hence, the current work was conducted to investigate the hot deformation behavior of AISI 403 that is one of the most applicable martensitic stainless steels.

2. Experimental Procedures

The chemical composition of AISI 403 martensitic stainless steel used in this study is given in Table 1. Cylindrical specimens with 10 mm in diameter and 12 mm in height were prepared from an as-received hot forged bar according to the ASTM E209 standard. To get a homogeneous austenitic structure before testing, all samples were reheated at 1200 ˚C for 15 min. Figure 1 shows optical micrograph of the annealed sample before testing with an average prior austenite grain size of about 80 μm.

Table 1. Chemical composition of AISI 403 martensitic stainless steel used in present investigation.

Element	C	Cr	Ni	Mn	Si	S	P	Fe
Wt.%	0.11	12.64	0.86	0.86	0.37	0.01	0.04	Bal.

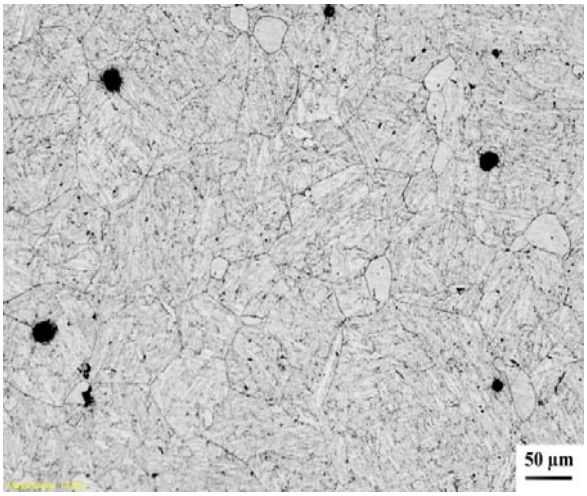

Fig. 1. Starting microstructure of AISI 403 martensitic stainless steel used in this research after reheating.

After austenitizing, samples were cooled down to deformation temperatures over range of 900 ˚C -1200 ˚C (in steps of 100 ˚C) held for 3 minutes and then subjected to hot compression at four various strain rates (0.001 s^{-1}, 0.01 s^{-1}, 0.1 s^{-1} and 1 s^{-1}) up to true strain of 0.8. Deformed specimens were immediately

quenched (in less than 3 s) in cold water to freeze the microstructure of hot deformation. A Zwick/Roell testing machine was used to perform hot compression tests. The thermomechanical treatment performed on specimens is drawn schematically in Fig. 2. The quenched specimens were subsequently cut in longitudinal direction, ground and polished according to the standard ASTM E3-11 and finally etched in ammonium persulfate and chloridric acid etchant to reveal the prior austenite grain boundaries. Optical microscopy observations were performed using an Olympus X51 microscope. The grain size measurements of the deformed samples were carried out according to ASTM E112-13 standard.

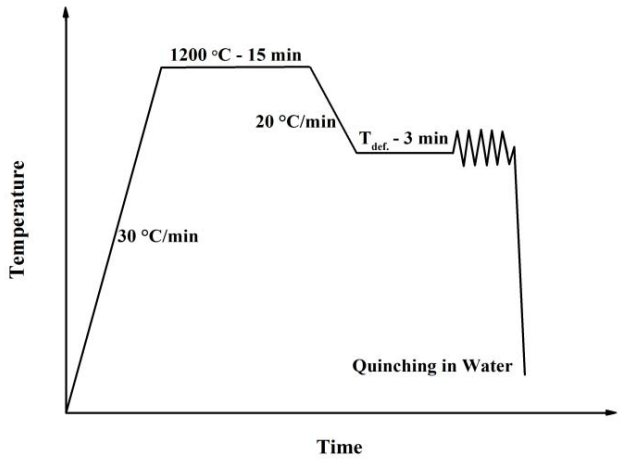

Fig. 2. Schematic representation of thermomechanical treatment performed on specimens in this study.

3. Results and Discussion

3.1. Analyzing flow curves

Figure 3 shows the representative true stress-true strain curve of the studied material at 1000 ·C and at a strain rate of 0.01 s^{-1}. The curve is clearly typical of DRX with a single peak after which flow softening reduces the flow stress down to the steady state condition. To study the mechanism of microstructural evolution, the same test was repeated with four consecutive strains of 0.2, 0.4, 0.6 and 0.8 and the deformed samples were immediately quenched after testing. The strains were chosen in a way to help analyze the microstructure at different regions of the flow curve as well below the peak (point A), around the peak (point B), flow softening (point C) and the steady state condition (point D). The microstructures corresponding to the points denoted by letters A, B, C and D on the flow curve are presented in Fig. 4. It is obvious from Fig. 4(a) that at strains well below the peak (e.g. point A) work hardening is dominant and the initial grains are deformed and elongated along the compression axes. In the strain region between points A (ε=0.2) and B (ε=0.4) which is beyond the peak, primary DRX grains are formed and work hardening descends. Figure 4(b) shows the presence of fine grains produced by recrystallization in the vicinity of the initial grain boundaries of work hardened grains. It is worth mentioning that the new grains are mostly observed around the grain boundaries where strain is more concentrated. Figure 4(c) and 4(d) illustrates that by increasing strain to 0.6 and further to 0.8, recrystallization develops to a fully equiaxed recrystallized grain structure at the onset of the steady state region.

The results of hot compression tests under different deformation conditions are shown in Fig. 5. It is clear that over the whole studied temperature and strain rate that ranges the hot deformation behavior of the material is controlled by work hardening and DRX. It is inferred that the hot deformation behavior is

remarkably affected by the deformation parameters. As expected, the flow stress level increases as the deformation temperature declines or strain rate rises. At high temperatures the increase in the rate of flow softening is associated with increasing the mobility of dislocations and grain boundaries. This, in turn, increases the nucleation and growth rates of DRX. The decrease in strain rate has a positive effect on the flow softening because it extends the deformation time and favors more development of DRX.

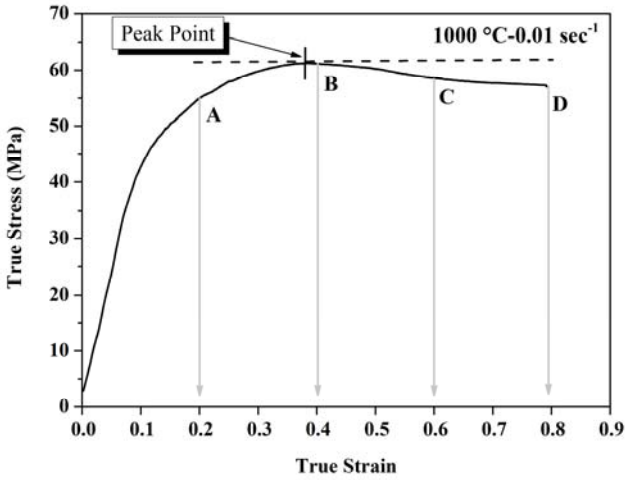

Fig. 3. Typical true stress-strain curve of 403 stainless Steel at 1000 °C and at a strain rate of 0.01 s-1.

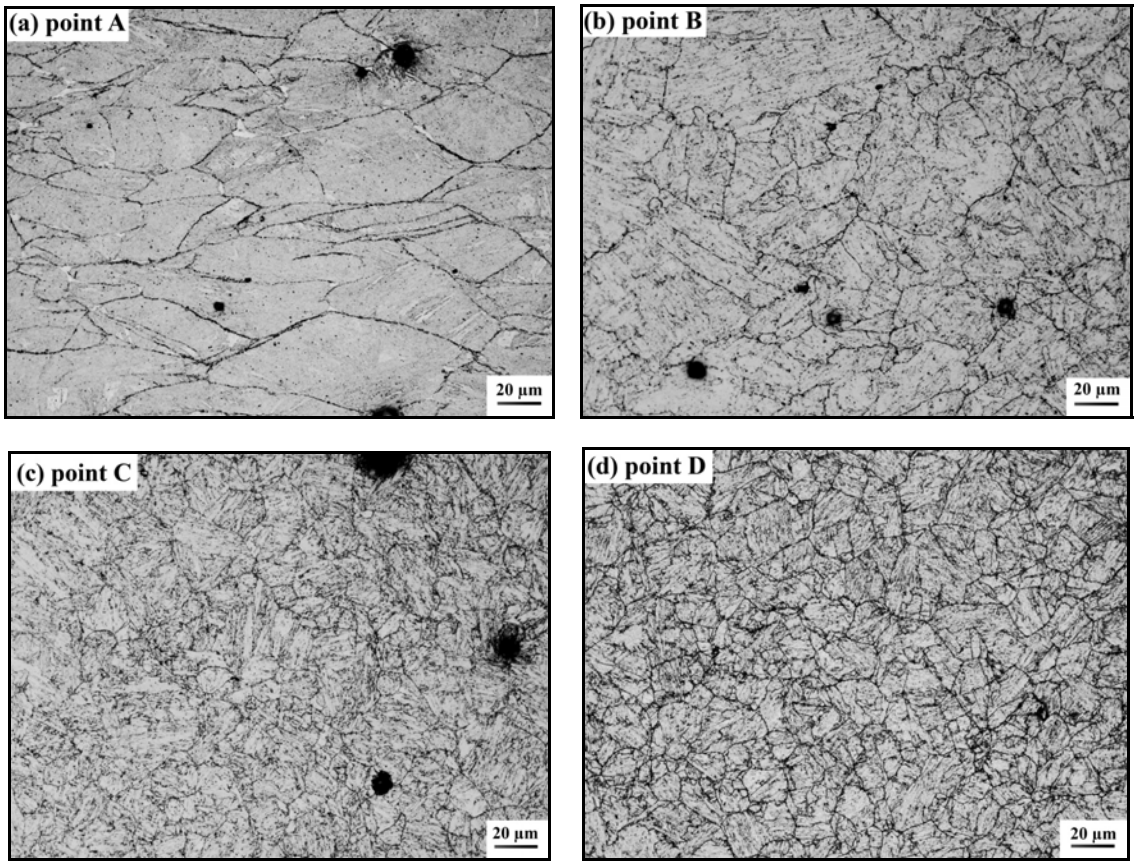

Fig. 4. Micrographs of hot deformed samples at 1000 °C and strain rate of 0.01 s^{-1} to different strains of (a) 0.2, (b) 0.4, (c) 0.6 and (d) 0.8.

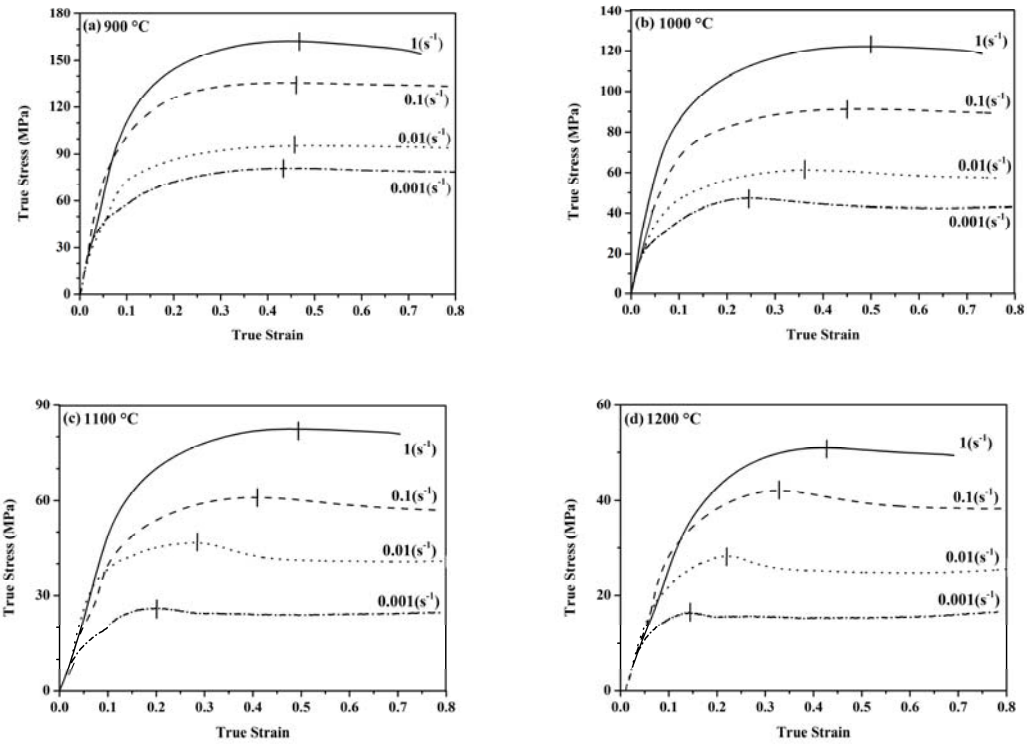

Fig. 5. True stress-strain curves under different hot deformation conditions, (a) 900 °C, (b) 1000 °C, (c) 1100 °C and (d) 1200 °C.

As indicated by Figs. 3 and 4, DRX becomes completed at the onset of the steady state region. As in this region, the work hardening and softening rates equal establishing this condition requires the completion of DRX and hence it is not well recognized at low deformation temperature and high strain rates.

3.2. Hot deformation characteristic points

It is well known that the peak of flow curve is a reliable measure of the starting point of DRX. However, in reality, DRX actually initiates at a critical strain well below the peak. It has been reported that the critical strain can be readily derived from the variation of work hardening rate versus the flow stress [10, 11, 13]. Figure 6 shows the plot of work hardening rate ($\theta=d\sigma/d\varepsilon$) against the true stress under different deformation conditions, according to the method that was originally proposed by Poliak and Jonas [10]. The inflection point on the work hardening plots vs. true stress corresponds to the initiation of DRX that is termed as the critical point and its strain and stress are known as the critical strain (ε_c) and stress (σ_c), respectively. As seen, increasing temperature and decreasing strain rate shifts the inflection (critical) point of the curve to the lower positions in terms of stress and strain.

For industrial applications, it is very useful to relate the characteristic points of the flow curves to the deformation conditions using simple equations. In similar researches simple power equations have been used to correlate the characteristic strains and stresses with the deformation variables of temperature and strain rate [16]. In such equations, the effects of temperature and strain rate are often incorporated in the Zener-Holloman parameter, as follows:

$$Z = \dot{\varepsilon}\exp(\frac{Q}{RT}) \quad (1)$$

where, Z denotes the Zener-Holloman parameter, $\dot{\varepsilon}$ is the strain rate (s^{-1}), T is the absolute deformation temperature (K), R is the gas constant (8.314 J mol^{-1} K^{-1}) and Q is the activation energy of deformation (kJ mol^{-1}). The value of activation energy at the peak point for a type of steel similar to that of the present study has been reported to be 448 kJ mol^{-1} [17]. In a work performed by Ren et al. [18], Q was determined as a function of strain and its value around the peak of flow curves was close to the value taken here. The dependence of characteristic points on the deformation condition can be established using the Zener-Hollomon parameter, as presented in Fig. 7. It is evident that the decrease in Z (i.e. increasing temperature or decreasing strain rate) shifts all the characteristic points to lower stresses and strains. This stems from the fact that increasing temperature and decreasing strain rate facilitate the condition for the occurrence of DRX. The following relationships between the Zener-Holloman parameter and the characteristic points can be derived from the results presented in Fig. 7:

$$\sigma_P = 9.032\mathrm{Ln}(Z) - 267.54 \quad (2)$$

$$\varepsilon_P = 0.0259\mathrm{Ln}(Z) - 0.59 \quad (3)$$

$$\sigma_C = 7.94\mathrm{Ln}(Z) - 236.86 \quad (4)$$

$$\varepsilon_C = 0.0125\mathrm{Ln}(Z) - 0.28 \quad (5)$$

$$\sigma_S = 7.022\mathrm{Ln}(Z) - 200.14 \quad (6)$$

$$\varepsilon_S = 0.0456\mathrm{Ln}(Z) - 1.12 \quad (7)$$

where, subscripts "C", "P" and "S" refer to critical, peak and steady state, respectively. In this work the ratio of σ_c/σ_p during hot deformation was found to be nearly constant as 0.84. This value is in good agreement with other reports in the literature [14, 15].

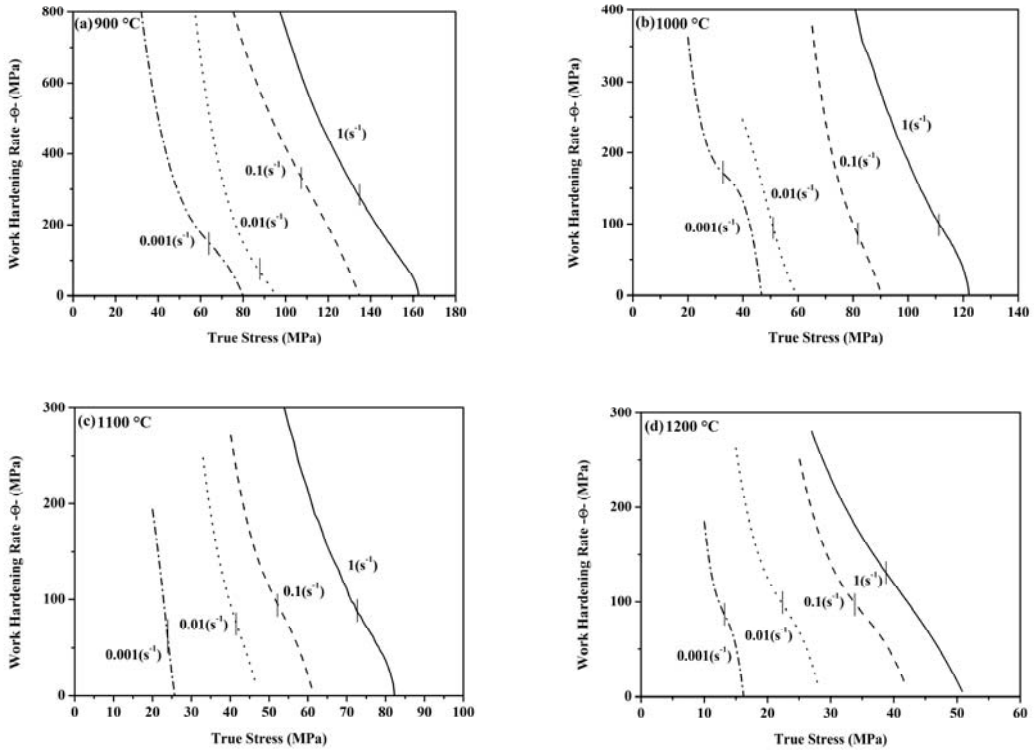

Fig. 6. Work hardening rates versus true stress at different hot deformation conditions, (a) 900 °C, (b) 1000 °C, (c) 1100 °C and (d) 1200 °C.

3.3. Dynamic recrystallization kinetics

Dynamic recrystallization proceeds with strain and its kinetics depends on strain rate and temperature.

Optical micrographs of the samples deformed at strain rate of 0.001 s^{-1} and temperatures of 900 °C, 1000 °C, 1100 °C and 1200 °C are presented in Fig. 8. The micrograph obtained at 900 °C (Fig. 8(a)) shows that the DRX new grains have formed almost along the prior grain boundaries and have occupied more than 50 % of the deformed matrix. As the temperature increases to 1000 °C (Fig. 8(b)), the DRX fraction grows and only sparse regions of deformed grains remain. At high temperatures, i.e. 1100 ·C and 1200 ·C, the microstructure is fully recrystallized reflecting accelerating DRX with increasing temperatures. It is also notable that increasing deformation temperature has sharply increased the tendency for grain growth, so that the average grain size of the DRX grains that was about 15 micron at 900·C increases to 25, 45 and 55 micron at 1000 ·C, 1100 ·C and 1200 ·C, respectively.

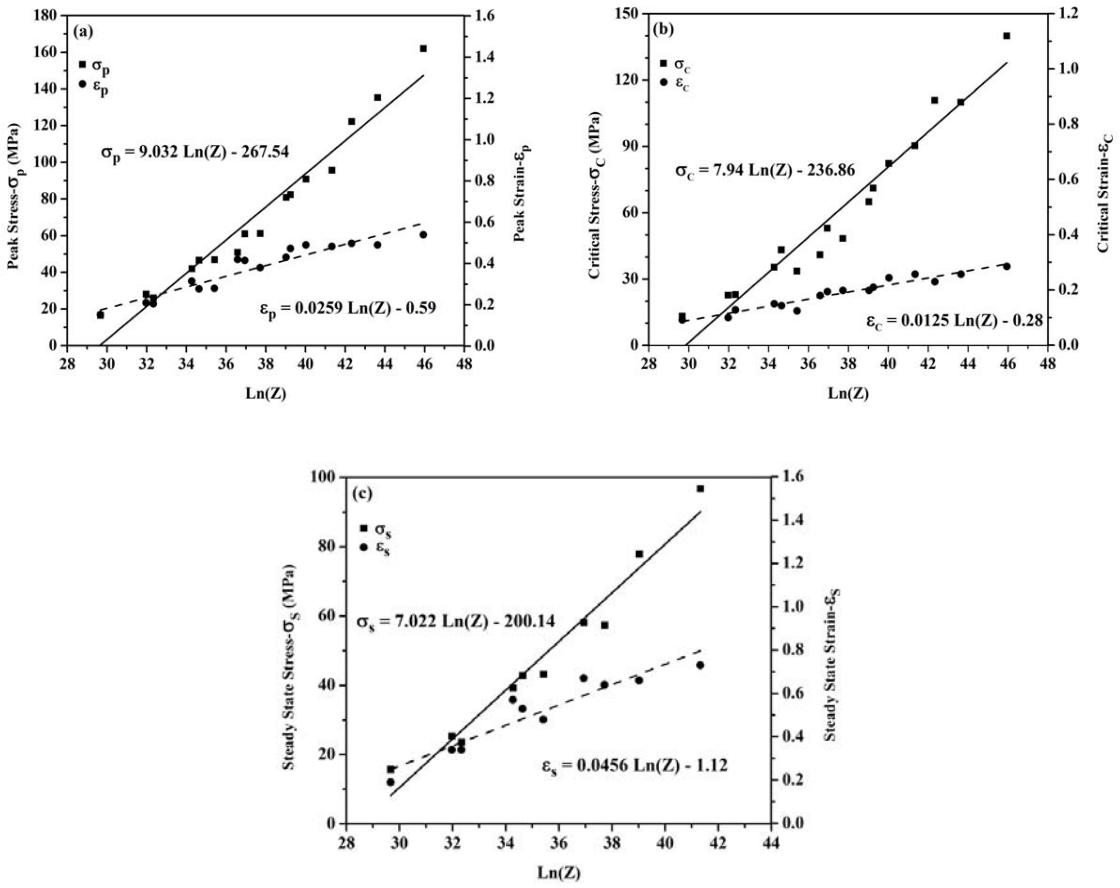

Fig. 7. Characteristic stress and strain of (a) peak point, (b) critical point and (c) steady state point as functions of Zener-Holloman parameter.

The variation of fraction recrystallized with increasing strain is observed in Fig. 9. It can be seen that DRX fraction increases with increasing temperature and decreasing strain rate. For instance, the DRX fraction in Fig. 9(a) (900 °C) is lower at all studied strain rates comparing to higher temperatures. Rather, it is observed that at low temperatures, e.g. 900 °C, DRX is completed at strains well beyond the total strain of 0.8 applied in the current tests. On the other hand, at high temperatures and low strain rates, e.g. 1200 °C and 0.001 s^{-1}, DRX becomes completed at lower strains.

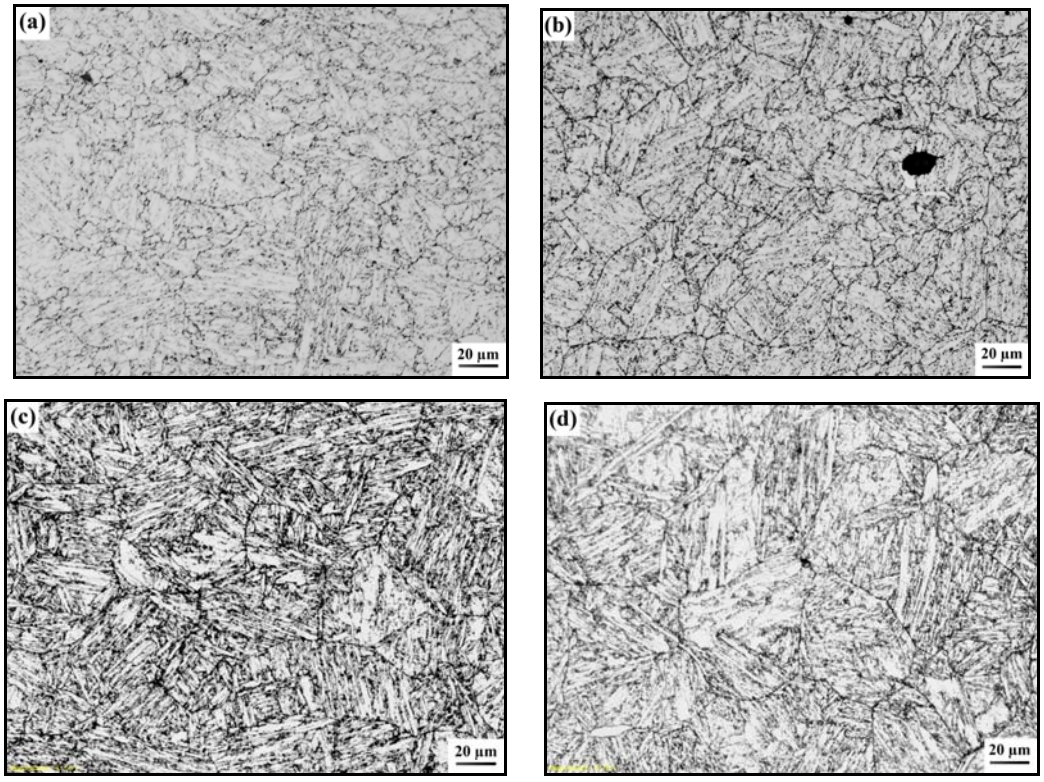

Fig. 8. Optical micrographs of samples deformed at strain rate of 0.001 s^{-1} and temperatures of (a) 900 °C, (b) 1000 °C, (c) 1100 °C, and (d) 1200 °C.

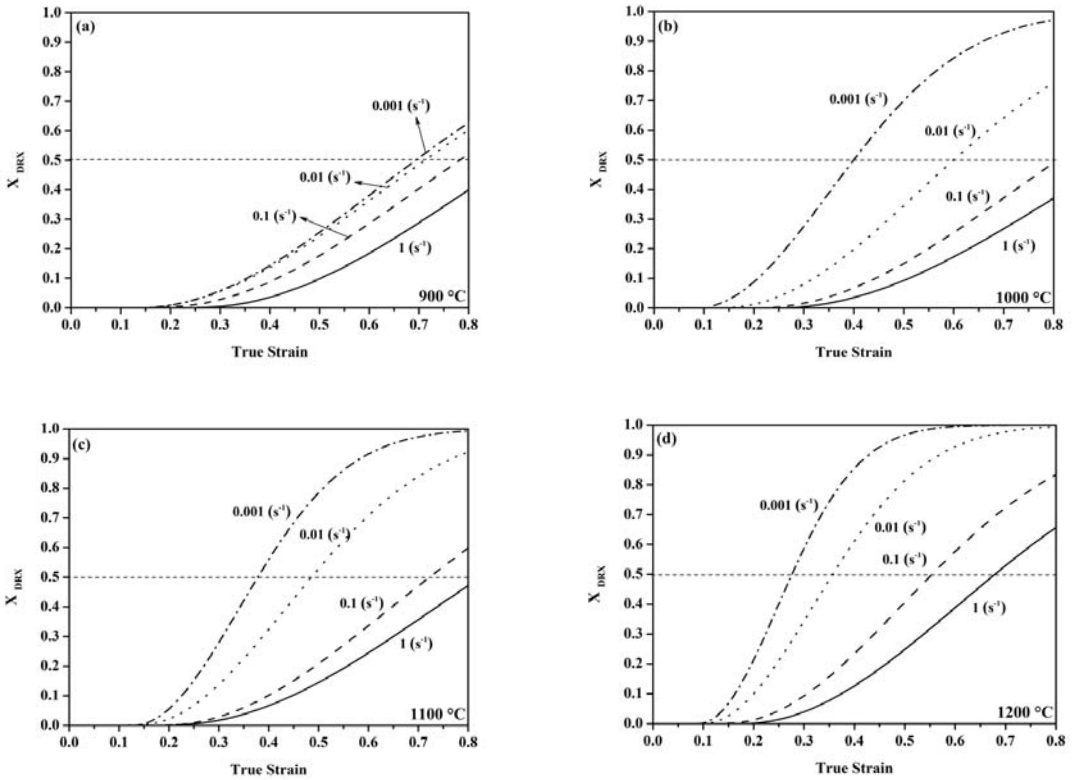

Fig. 9. Variation of dynamic recrystallization fraction with strain at different deformation conditions, (a) 900 °C, (b) 1000 °C, (c) 1100 °C and (d) 1200 °C.

The relationship between the volume fraction of DRX and strain during hot deformation can be readily described by different experimental or physics-based equations [5, 14, 19, 20]. The Avrami kinetics equation is often used to describe the fraction recrystallized (X_{DRX}) as a function of deformation time, given by:

$$X_{DRX} = 1 - \exp(-kt^{-n}) \tag{8}$$

where, k and n are the material constants. As DRX progresses with strain, the above equation can be rewritten as follows [16].

$$X_{DRX} = 1 - \exp(-0.693(\frac{\varepsilon - \varepsilon_C}{\varepsilon_{50\%}})^2) \tag{9}$$

where, ε is instant true strain, ε_c is the critical strain and $\varepsilon_{50\%}$ is the strain required for 50 percent recrystallization. The values of $\varepsilon_{50\%}$, $\varepsilon_{10\%}$ (10% recrystallization) and $\varepsilon_{90\%}$ (90% recrystallization) determined from the curves of Fig. 9 have been drawn in Fig. 10 as functions of Z at different deformation conditions. It is clearly observed that increasing Z results in shifting $\varepsilon_{10\%}$, $\varepsilon_{50\%}$ and $\varepsilon_{90\%}$ to higher values. The linear regression of the data points gives the following applied equations:

$$\varepsilon_{10\%} = 0.0215\text{Ln}(Z) - 0.46 \tag{10}$$

$$\varepsilon_{50\%} = 0.0355\text{Ln}(Z) - 0.78 \tag{11}$$

$$\varepsilon_{90\%} = 0.0511\text{Ln}(Z) - 1.07 \tag{12}$$

In a similar approach Zeng et al. [21] reported that the Avrami kinetics equation can be used for case of DRX in AISI 403Nb alloy. They reported a value of 2.3 for the Avrami exponent (n) and represented power-law equations for the dependence of peak and critical strains on Z.

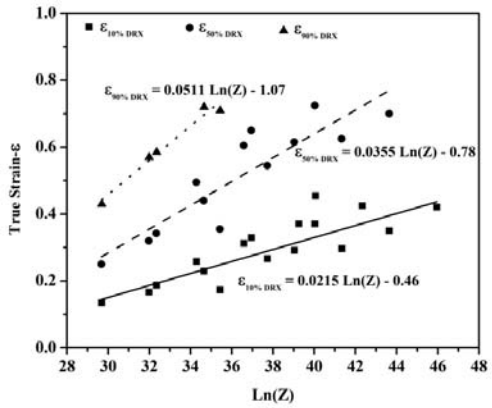

Fig. 10. Variation of the strains required for 10%, 50% and 90% dynamic recrystallization ($\varepsilon_{10\%}$, $\varepsilon_{50\%}$ and $\varepsilon_{90\%}$) fraction with the Zener-Hollomon parameter.

3.4. Modeling flow curves

Many attempts have been devoted to develop a formalism for σ(ε). Different approaches of empirical, semi-empirical and physical-based have been used in the literature to predict flow stress at the early stages of DRX [22-24]. The flow stress up to the completion of DRX at the steady state region is very crucial particularly from the industrial point of view. This is because the steady state flow stress (σ_s) is constant at a given deformation condition and can be simply predicted by a power-law equation as proposed in Eq. 6. Due to the complexity of physical-based equations, more simple experimental descriptions of σ(ε) are

solicited for industrial applications. In this way, Baragar [25] proposed a power equation for plain carbon and low alloy steels as follows:

$$\sigma = b + c\varepsilon^{0.4} + d\varepsilon^{0.8} + e\varepsilon^{1.2} \tag{13}$$

where, b, c, d and e are constants. Although this equation has been successfully used for plain carbon and low alloy steels, the four constants seems to be dependent on the deformation condition and the powers may vary for different alloys. In order to modify Eq. 13, it is possible to use another experimental equation proposed by Cingara and McQueen [26] as follows:

$$\frac{\sigma}{\sigma_p} = [(\varepsilon/\varepsilon_p)\exp(1-\varepsilon/\varepsilon_p)]^C \tag{14}$$

where, C is a material constant and σ_P and ε_p denotes the stress and strain of the peak point. Using the Tylor series for the exponential function ($\exp(x) = 1+x+x^2/2!+\ldots$) and doing some algebraic operations, Eq. 14 can be simplified as follows:

$$\frac{\sigma}{\sigma_p} = \left[2.5\left(\frac{\varepsilon}{\varepsilon_p}\right) - 2\left(\frac{\varepsilon}{\varepsilon_p}\right)^2 + 0.5\left(\frac{\varepsilon}{\varepsilon_p}\right)^3\right]^C \tag{15}$$

By developing the right-hand side of above equation and neglecting some terms for simplicity, Eq. (15) can be simplified to take the form of Baragar's equation as follows:

$$\sigma = \sigma_P\left[2.5\left(\frac{\varepsilon}{\varepsilon_p}\right)^C - 2\left(\frac{\varepsilon}{\varepsilon_p}\right)^{2C} + 0.5\left(\frac{\varepsilon}{\varepsilon_p}\right)^{3C}\right] \tag{16}$$

This equation is more applicable than Eq. (13) because the coefficients are constant and σ_P and ε_P determine the dependence on deformation temperature and strain rate as in Eqs. (2) and (3). The value of C can be determined by plotting the experimental data in a logarithmic scale. Hence, half of experimental data at 900°C and 1200°C were used to determine the average value of C as 0.7 in Fig. 11 and the rest of flow curves at 1000°C and 1100°C were used to verify the model. Fig. 12 shows that Eq. (16) successfully predicts the flow curves of the material up to the steady state region with a good precision. Therefore, Eqs. (2), (3), (6), (7) and (16) can be combined to completely draw flow curves of the material at various deformation conditions.

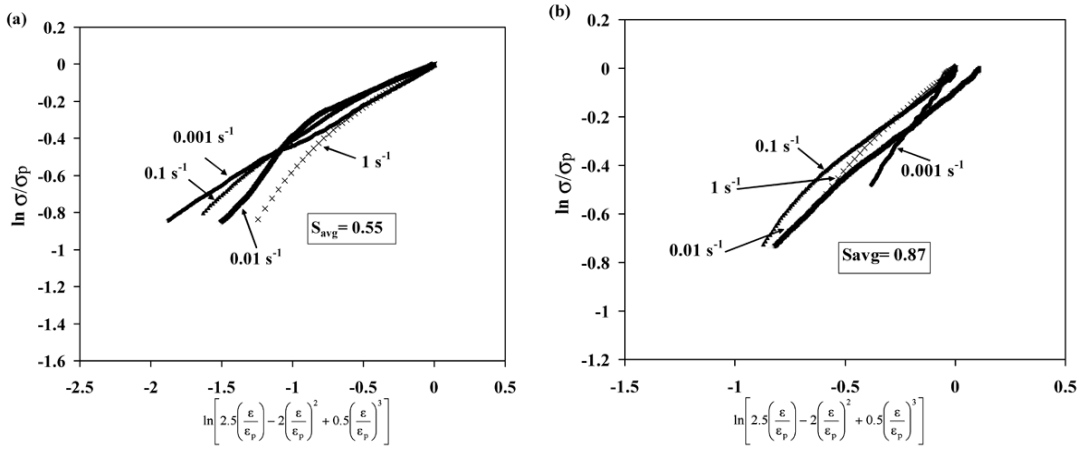

Fig. 11. Variation of normalized flow stress with normalized flow strain at different strain rates and temperatures of (a) 900 °C, (b) 1200 °C. S_{avg} is the average slope of the curves and corresponds to C in Eqs. (15) and (16).

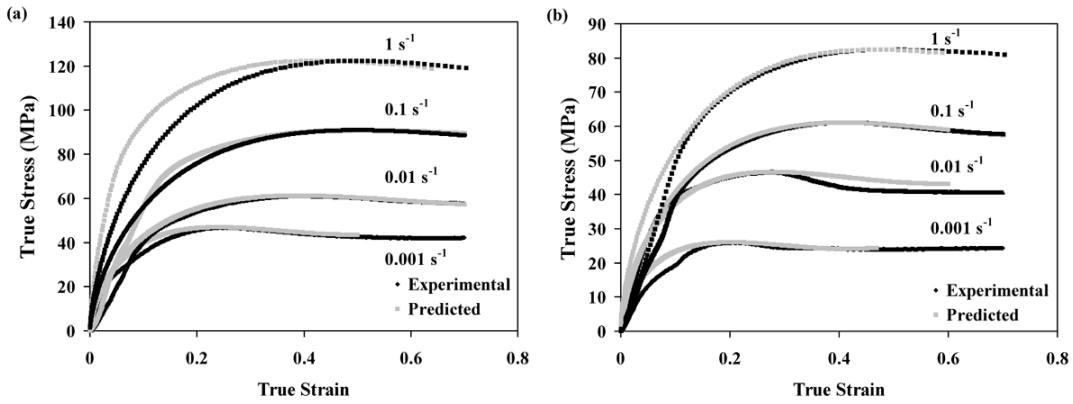

Fig. 12. Comparison of the experimental data with the modeling curves predicted by Eq. (16) at various strain rates and temperatures of (a) 1000 °C and (b) 1100 °C.

4. Conclusion

In this work, the dynamic recrystallization behavior of AISI 403 martensitic stainless steel was investigated using hot compression tests conducted at temperature range of 900°C -1200 °C and at strain rate range of $0.001s^{-1}$-1 s^{-1}. The major results can be summarized as follows:

(1) All of the flow curves represented the occurrence of dynamic recrystallization with the typical single peak behavior.

(2) The stress and strain corresponding to the critical, peak and steady state region were related to the Zener-Hollomon parameter using simple power equations.

(3) The variation of dynamic recrystallization fraction with strain was depicted according to the Avrami kinetics equation. It was predicted that dynamic recrystallization was partial at all strain rates at 950 ·C. However, at 1200 ·C, partial dynamic recrystallization was obtained at 0.1 and 1 s^{-1}.

(4) In order to model all parts of a typical flow curve, the equation proposed by Cingara-McQueen was modified by the Baragar's equation. The modified equation in form of $\sigma = \sigma_P[2.5(\varepsilon/\varepsilon_p)^{0.7} - 2(\varepsilon/\varepsilon_p)^{1.4} + 0.5(\varepsilon/\varepsilon_p)^{2.1}]$ could predict the flow curves up to the onset of steady state flow region.

5. References

[1] M. Mirzaee, H. Keshmiri, G.R. Ebrahimi and A. Momeni, Dynamic recrystallization and precipitation in low carbon low alloy steel, 26NiCrMoV 14-5, *Materials Science and Engineering*, A 551 (2012) 25-31.

[2] T. Yan, E. Yu and Y. Zhao, Constitutive modeling for flow stress of 55SiMnMo bainite steel at hot working conditions, *Materials Design*, 50 (2013) 574-580.

[3] H. Dehghan, S.M. Abbasi, A. Momeni and A. Karimi Taheri, On the constitutive modeling and microstructural evolution of hot compressed A286 iron-base superalloy, *Journal of Alloys and Compounds*, 564 (2013) 13-19.

[4] A. Momeni, K. Dehghani, M. Heidari and M. Vaseghi, Modeling the flow curve of AISI 410 martensitic stainless steel, *Journal of Materials Engineering Performance*, 21 (2012) 2238-2243.

[5] A. Momeni, K. Dehghani, and G.R. Ebrahimi, Modeling the initiation of dynamic recrystallization using a dynamic recovery model, *Journal of Alloys and compounds*, 509 (2011) 9387-9393.

[6] W. Bang, C.S. Lee and Y.W. Chang, Finite element analysis of hot forging with flow softening by dynamic recrystallization, *Journal of Materials Processing Technology*, 134 (2003) 153-158.

[7] J. Huang and Z. Xu, Evolution mechanism of grain refinement based on dynamic recrystallization in multiaxially forged austenite, *Materials Letter*, 60 (2006) 1854-1858.

[8] L. Sahebdel, S.M. and Abbasi, A. Momeni, Microstructural evolution through hot working of the single-phase and two-phase Ti-6Al-4V alloy, *International Journal of Materials Research*, 102 (2011) 1-7.

[9] L. Wang, F. Liu, Q. Zuo and C.F. Chen, Prediction of flow stress for N08028 alloy under hot working conditions, *Materials Design*, 47 (2013) 737-745.

[10] E.I. Poliak and J.J. Jonas, A one-parameter approach to determining the critical conditions for the initiation of dynamic recrystallization, *Acta Materialia*, 44 (1996) 127-136.

[11] A. Momeni and K. Dehghani, Microstructural evolution and flow analysis during hot working of a Fe-Ni-Cr superaustenitic stainless steel, *Metallurgical and Materials Transactions*, A42 (2011) 1925-1932.

[12] G.R. Ebrahimi, A. Momeni, M. Jahazi and P. Bocher, Dynamic recrystallization and precipitation in 13Cr super-martensitic stainless steels, *Metallurgical and Materials Transactions*, A45 (2014) 2219-2231.

[13] G.R. Ebrahimi, H. Keshmiri, A. Momeni and M. Mazinani, Dynamic recrystallization behavior of a superaustenitic stainless steel containing 16%Cr and 25%Ni, *Materials Science and Engineering*, A528 (2011) 7488-7493.

[14] J.J. Jonas, X. Quelennec, L. Jiang and E. Martin, The Avrami kinetics of dynamic recrystallization, *Acta Materialia*, 57 (2009) 2748-2756.

[15] A. Momeni, S.M. Abbasi and H. Badri, Hot deformation behavior and constitutive modeling of VCN200 low alloy steel, *Applied Mathematical Modeling*, 36 (2012) 5624- 5632.

[16] S. H. Cho and Y. C. Yoo, Hot rolling simulations of austenitic stainless steel, *J. Mater. Sci*. 36 (2001) 4267-4272.

[17] A. Momeni, K. Dehghani, G.R. Ebrahimi and H. Keshmiri, Modeling the flow curve characteristics of 410 martensitic stainless steel under hot working condition, *Metallurgical and Materials Transactions*, A41 (2010) 2898-2904.

[18] F. C. Ren, J. Chen and F. Chen, Constitutive modeling of hot deformation behavior of X20Cr13 martensitic stainless steel with strain effect, *Transaction of Nonferrous Metals Society of China*, 24 (2014) 1407-1413.

[19] S. L. Semiatin, G. Damamme, D. Piot and F. Montheillet, Report No. AFRL-RX-WP-TP-2009-4117, Air Force Research Laboratory, USA, (2009).

[20] G.R. Ebrahimi, H. Keshmiri, A. Maldad and A. Momeni, Dynamic recrystallization behavior of 13%Cr martensitic stainless steel under hot working condition, *Journal of Materials Science and Technology*, 28 (2012) 467-473.

[21] Z. Zeng, L. Chen, F. Zhu and X. Liu, Dynamic recrystallization behavior of a heat-resistant martensitic stainless steel 403Nb during hot deformation, *Journal of Materials Science and Technology*, 27 (2011) 913-919.

[22] P. Bernard, S. Bag, K. Huang and R.E. Loge, A two-site mean field model of discontinuous dynamic recrystallization, *Materials Science and Engineering*, A528 (2011) 7357-7367.

[23] A. Momeni, G.R. Ebrahimi, M. Jahazi and P. Bocher, Microstructure evolution at the onset of discontinuous dynamic recrystallization: A physics-based model of subgrain critical size, *Journal of Alloys and Compounds*, 587 (2014) 199-210.

[24] Z. Zeng, S. Jonsson, H. Jørgen Roven and Y. Zhang, Modeling the flow stress for single peak dynamic recrystallization, *Materials Design*, 30 (2009) 1939-1943.

[25] D.L. Baragar, The high temperature and high strain-rate behavior of a plain carbon and HSLA steel, *Journal of Mechanical Working Technology*, 14 (1987) 295-307.

[26] Cingara and H.J. McQueen, New formula for calculating flow curves from high temperature constitutive data for 300 austenitic steels, *Journal of Materials Processing Technology*, 36 (1992) 31-42.